Field desorption of lithium

Yu. Suchorski,* V. K. Medvedev,† and J. H. Block
Fritz-Haber-Institut der Max-Planck-Gesellschaft, Faradayweg 4-6, 14195 Berlin, Germany

R. L. C. Wang and H. J. Kreuzer
Department of Physics, Dalhousie University, Halifax, Nova Scotia, Canada B3H 3J5
(Received 27 June 1995)

Absolute appearance energies of field-desorbed Li^+ ions were obtained from mass-to-charge resolved retarding potential analyses of Li^+ emitted from the first and second Li layer on W(111). Activation energies for Li^+ field desorption were derived from desorption rate measurements. The field-independent binding energy of Li adatoms has been found from field-dependent Li^+ appearance and activation energy values, indicating a negligible field-induced charge transfer in the applied field range. We use the cluster embedded in jellium model, based on density-functional theory, to interpret the data by calculating local field enhancements, surface potentials, and activation energies for Li field desorption as a function of field strength and surface coverage as well as geometry.

I. INTRODUCTION

Adsorption and desorption on solid surfaces is greatly influenced by the local environment of the adsorbed particle in that the surface structure and the coordination of the adsorption site determine the energetics, vibrational properties, and ultimately its chemistry. Lateral interactions effect the local environment as the coverage increases and leads, as an example, to an increase or a decrease in the heat of adsorption depending on whether the lateral interactions are predominantly attractive or repulsive.

Electrostatic fields of a few volts per angstrom effect the local environment of an adparticle dramatically in that they alter the electronic structure in the surface region. As an example they will (field) desorb atoms and molecules from a metal surface even at such low temperatures where field-free thermal desorption is inefficient.[1]

The interplay between adsorption and desorption on metal surfaces and (locally varied) applied electrostatic fields is very complex as it is ultimately the consequence of the self-consistent arrangement of the electrons in the surface region. In this paper we present a detailed study, both experimental and theoretical, of the field desorption of Li from a transition-metal surface looking in particular at the site specificity and the coverage dependence.

Field desorption of alkalis has been extensively studied in the past, establishing the surface specificity and also the increase of the externally applied desorption field as a function of coverage.[2–6] Two explanations have been advanced: (i) an increase in coverage results in an increase of the activation energy of field desorption, which must be compensated by an increase in the applied field strength,[2–6] and (ii) an increase in coverage leads at the constant applied field to a decrease of the local field, which must be externally compensated.[7] We will see that these different facets of field desorption are ultimately linked and a consistent picture can only be derived from a microscopic theory. We will also show that experimental difficulties with obtaining the local desorption fields and with deriving binding energies of the alkali adatoms for selected surface sites from field desorption measurements can be overcome using a new experimental approach based on the retarding potential analysis of field-desorbed alkali ions.[8] This approach is based on the measurements of absolute field ion appearance energies of the field-desorbed metal ions and activation energies of field desorption. We have previously reported first successful attempts to analyze Li^+ ions field desorbed from a two-layer Li film in such experiments.[8] In the present study this experimental approach is extended towards the Li monolayer.

Because there is a certain amount of confusion in the use of concepts like local fields, activation, and binding energies, etc., we begin our discussion in the next section with some definitions, also presenting experimental results. We will then, in Sec. III, report results on the local field at specific surface sites and as a function of Li coverage. Section IV presents more theoretical results on activation energies and desorption fields and Sec. V is devoted to a thorough discussion of the experimental findings in the light of these theoretical results.

II. EXPERIMENTAL STUDY OF FIELD DESORPTION OF Li FROM W

A. Preliminaries

Field-desorbed particles are always ions whereas in *thermal desorption* they are often neutral particles. It is therefore important to consider the effective potential-energy surfaces seen by an adparticle as it leaves the surface as an ion. In quantum mechanics we can calculate adiabatic energy surfaces representing the energy of the system for fixed positions of the ionic cores. The ground-state energy curve, depicted in Fig. 1, represents the holding potential for an adsorbed atom. As we move the adsorbed atom away from the potential minimum there will come a point where the highest occupied electronic level in the atom will move above the Fermi energy of the metal leading to charge draining. In a crude approximation we can say that an ion of charge q is formed at or just beyond the Schottky hump,

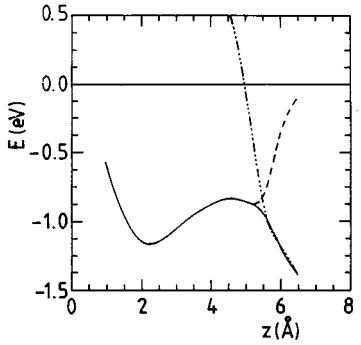

FIG. 1. Potential energy, defined in (7), of a Li adatom as a function of distance perpendicular to the surface for adsorption of a single Li atom on a Li(5+4) cluster, geometry (a) Fig. 7, in the CEJ model for F_0=5 V/nm. Solid curve: ground-state energy. Dashed curve: lowest excited state.

which for larger distances, is accelerated away in an asymptotic field F_0. This picture however, conveys only half the story of thermal field desorption, namely, that the desorbing particle has to be activated thermally from the potential minimum to an energy above the Schottky hump. The activation energy, called field-desorption energy from now on, is therefore given by

$$E_{\mathrm{des}}(F_0)=E_{\mathrm{total}}(F_0,z_{\mathrm{crit}},M-A)-E_{\mathrm{total}}(F_0,z_B,M-A). \tag{1}$$

The position of the Schottky hump, z_{crit}, is the critical distance where the singly charged ions are formed during desorption, and z_B is the position of the adsorbed atom bound to the surface. To form an ion an electron must be transferred from the desorbing particle to the metal by a tunneling process. This can only be described properly by taking into account exited states of the system of which the lowest is also shown in Fig. 1. From these adiabatic states one can construct diabatic states that correspond to asymptotically free neutral atoms and ions approaching the metal without undergoing ionization or neutralization at the Schottky hump, as shown in Fig. 1. The transition-matrix elements between these diabatic states are nonzero only in the vicinity of the Schottky hump and describe the tunneling process. It is interesting to note that for this system the diabatic states do not cross on top of the Schottky hump but slightly further away from the surface. As a result of such a calculation we get the rate of the thermal field desorption, which we can parametrize in the Arrhenius form to read

$$r_{\mathrm{des}}=\nu(\theta,T,F_0)\exp[-E_{\mathrm{des}}(\theta,F_0)k_BT], \tag{2}$$

where we indicated explicitly that both the prefactor (which can be factored into an attempt frequency in the surface potential and the tunneling probability) and the desorption energy are generally coverage and field dependent and the former also weakly temperature dependent. As the coverage in the adsorbate is increased the desorption energy increases or decreases depending on whether lateral interactions between adparticles are predominantly attractive or repulsive. The prefactor also depends on coverage because it is a measure of the entropy gain in the desorption process.

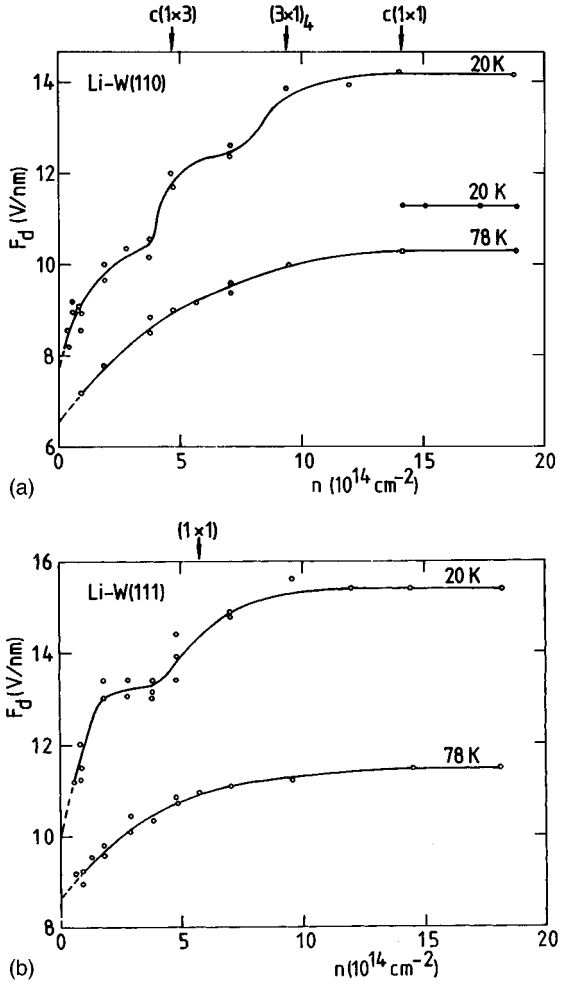

FIG. 2. (a) Experimental dependence of applied desorption field, F_d, for the (110) plane of a [110]-oriented W tip on the Li surface density of adatoms at tip temperatures of 20 and 78 K. The $c(1\times3)$, $(3\times1)_4$, and $c(1\times1)$ ordered Li structures are shown at their stoichiometric surface coverages (arrows). For the lower line at 20 K Li^+ ions desorb only from a topmost (second) Li layer whereas the W surface remains to be covered with a Li monolayer. (b) The same as in (a), but for the (111) plane of the same tip. Structure (1×1) is marked with an arrow.

As for the field dependence of the field-desorption energy we note that for systems, such as metals on metals, where the depth of the potential well does not change dramatically as a function of field strength, the activation energy is a monotonically decreasing function of field strength. We can define the desorption field strength for heterogeneous systems and the evaporation field strength for homogeneous systems that field strength where the desorption energy goes to zero, i.e., where the Schottky hump disappears. Because field-desorption experiments are done at low but finite temperatures one need only require that the Schottky hump becomes so small that it can be overcome by thermally activated processes; i.e., the desorption energy must be within tens of k_BT. In Figs. 2(a) and 2(b) we show the measured dependencies of the applied desorption field on the surface density of Li adsorbed on the (110) and (111) planes of a [110]-oriented W tip at two different temperatures, 20 and 78 K. Notice in

particular the steplike rises in curves measured at 20 K at Li densities where $c(1\times3)$ and $(3\times1)_4$ ordered structures form on the (110) plane or (1×1) on the (111) plane, respectively.

B. Retarding potential analysis of field-desorbed Li^+ ions

The local mass-to-charge-resolved retarding potential analysis for field-desorbed ions is based on recent improvements in the techniques of measuring the appearance energy of field ions,[9] which now allow one to obtain the *absolute* value of this energy for field ions of gas atoms or molecules,[10] or even field-evaporated metal atoms.[11] However, to analyze field-desorbed alkali ions in a retarding potential experiment, a measurable continuous flux of such ions from the probed surface sites must be provided. This prerequisite was really not attainable and prevented the application of the appearance energy spectroscopy to alkali adlayers.

We have developed a novel experimental procedure that achieves a continuous flux of Li^+ ions field desorbed from the apex of a field emitter tip, providing Li^+ desorption rates that are sufficiently high for field-ion appearance energy analyses (Li^+ ion current up to 10^{-10} A). A similar procedure was recently used for the successful imaging of metal surfaces with Li^+ ions in the new lithium field-desorption microscope (Li FDM),[12] in which the surface of the metal tip is imaged by field-desorbed Li^+ ions. In this device, the continuous supply of Li atoms to imaged surface sites is achieved via field-assisted surface diffusion from a Li multilayer deposited on the shank of the field emitter. Lithium atoms field desorbed from the top of the tip are continuously replaced, providing in this way Li^+ desorption rates that are sufficient for the visualization of the surface in the continuous mode of imaging. The achieved brightness of the image in the Li FDM is comparable with the one in the field-ion microscope using Ne or He as imaging gases. After choosing specific sites of the surface, imaged by Li FDM, one can analyze the Li^+ ions emitted from these sites with the retarding potential technique in the probe hole experiment.[8] In these experiments kinetic energies of Li^+ ions, field desorbed from a few surface sites of the apex plane of a [111]-oriented W tip and mass-to-charge resolved in a magnetic sector field, were measured with the five-electrode electrostatic retarding potential analyzer.[13] The absolute appearance energies of Li^+ ions A_{Li} were determined from the equation

$$A_{Li} = \phi_R - e\,\delta^{on}_{Li}, \tag{3}$$

where ϕ_R is the effective work function of the retarder electrode and δ^{on}_{Li} is the voltage applied between retarder and field emitter, just sufficient to collect the first Li^+ ions (onset value of the field-ion retardation curve). The value of ϕ_R was obtained *in situ* from measurements of the $\delta^{on}_{Ne,150\ K}$, onset voltage for field-ionized Ne at the emitter temperature of 150 K and the same ion beam energy as for Li^+ (2000 eV). In this case the absolute appearance energy of Ne^+ is exactly equal to the ionization energy of Ne, I_{Ne}.[9] Thus, the value of ϕ_R can be easily obtained from the equation $I_{Ne} = \phi_R - e\,\delta^{on}_{Ne,150\ K}$. The calibration of the applied external field F was based on the standard value for the evaporation field strength of W(111).[14] The problem of the field strength dropping during the experiment due to the growing tip radii as a result of field evaporation[15] does not exist in the case of field desorption of Li from an overlayer, because Li is continuously replaced by surface diffusion and the tip itself is not affected by applied fields less than 1 V/Å in the case of W.

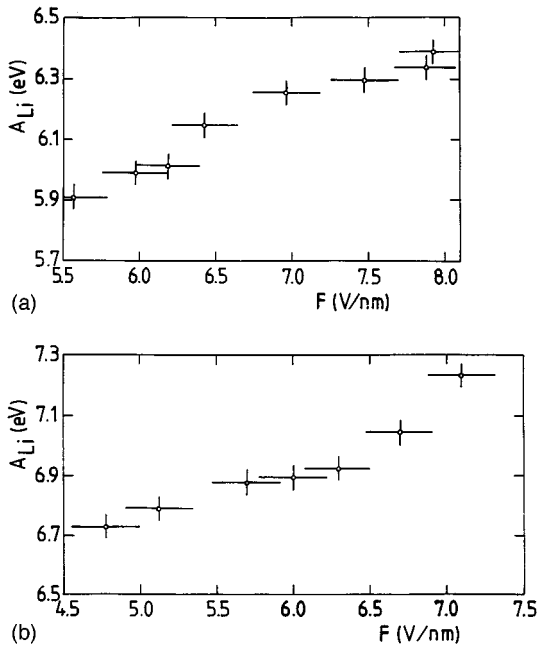

FIG. 3. (a) The dependence of experimentally determined appearance energy A_{Li} for Li^+ ions, field desorbed from the second Li layer on W(111), on the strength of externally applied field F. (b) The same as in (a) but for the Li^+ ions emitted from the Li monolayer.

Thus, the local mass-to-charge resolved retarding potential analyses for Li^+ and Ne^+ ions emitted from the same surface sites of W(111) allows us to obtain the absolute appearance energies for Li^+ ions emitted from the second, and (using monolayer Li deposit on the shank of the tip) first Li layer.

A significant field dependence of the experimentally determined appearance energy for Li^+ ions was observed for both desorption modes and is shown in Figs. 3(a) and 3(b). No temperature dependence of A_{Li} has been observed in the temperature range of 297–450 K, as expected from the analysis discussed in Ref. 13.

C. Evaluation of desorption energies

Desorption (activation) energies for field desorption of Li from W(111) were obtained from the temperature dependence of the Li^+ ion rates given by an Arrhenius analysis via Eq. (2). To minimize the effect of Li surface diffusion on the desorption rate, additional experiments using the pulse desorption mode of the Li FDM were performed. The details of the measurement and discussion concerning the influence of surface diffusion of Li on the $E_{des}(\theta,F_0)$ can be found elsewhere.[8] The experimental values of $E_{des}(\theta,F_0)$ for both *second layer* and *monolayer* modes of the Li field desorption are displayed in Figs. 4(a) and 4(b).

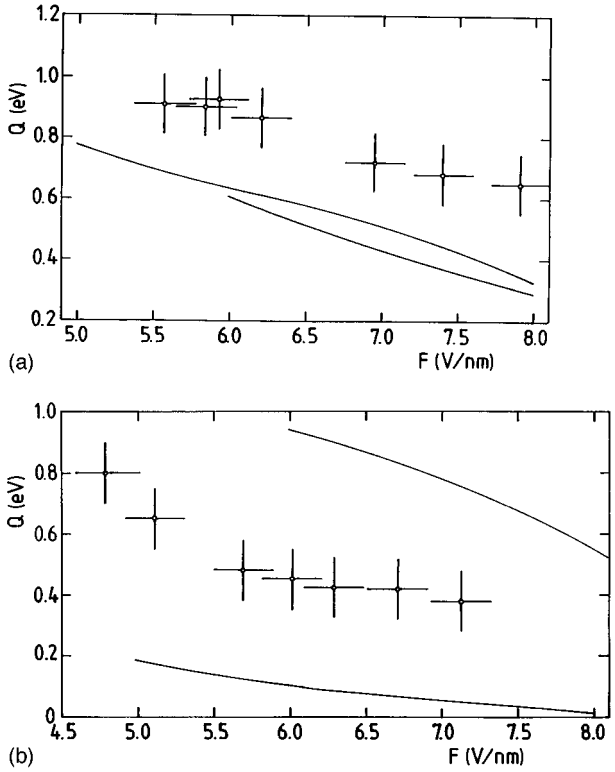

FIG. 4. (a) Experimentally determined activation energies Q_{ef} for field desorption of Li^+ from the second Li layer on W(111) as a function of externally applied field F. Also calculated curves are shown below as full lines: upper curve corresponds to Li adsorbed on a Li(5+4) cluster embedded in jellium, lower curve is for Li on jellium with $r_s=3.0$ bohr. (b) The same as in (a) but for a Li submonolayer. The upper full line gives the calculations for a Li atom adsorbed on the threefold hollow site of Mo(111) represented by a (3+3) cluster. The lower line is for Li in on top site of Mo(111) represented by a (3+1) cluster.

D. Derivation of binding energies

Based on the interpretation of the appearance energy of singly charged field-desorbed ions derived from the thermionic cycle[16] as

$$A_{\mathrm{Li}}(F)=I_{\mathrm{Li}}+\Lambda(F)-Q(F), \tag{4}$$

the binding energy $\Lambda(F)$ of the lithium atoms in the first and second Li layer on the W(111) surface can be easily obtained. No dependence of the binding energy of Li atoms on the externally applied electrostatic field is found within the experimental accuracy for both *second layer* and *monolayer* of Li on W(111). The field-independent values of 1.5 eV for the second Li layer and 2.05 eV for the Li monolayer, obtained from present experimental data, are in quantitative agreement with the corresponding field-free values for Li/W(111), obtained from lithium adsorption isobars (adsorption-desorption equilibrium measurements)[17] for the W(111) single-crystal plane (Fig. 5).

III. LOCAL-FIELD ENHANCEMENT

Before we report our calculations pertaining to adsorption and desorption of Li we would like to discuss briefly the concepts of local field and local-field enhancement.

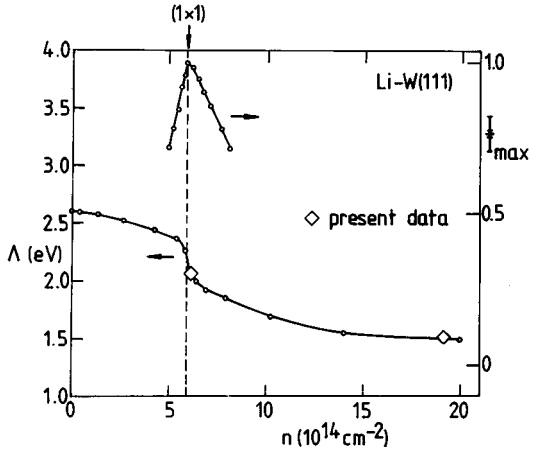

FIG. 5. Field-free binding energy, Λ, of Li adatoms on a W(111) single-crystal plane vs surface density of Li adatoms. Maximum of the intensity of low-energy electron diffraction spots, $I/I_{\max}$, corresponds to the structure (1×1) of Li adlayer. (After Ref. 17.)

An electrostatic field is the result of separating charges onto two metals by applying a voltage between them. If one of the metals is a tip with a radius of curvature of a few hundred angstroms then fields of the order of volts per angstrom can be generated in a region of a few hundred angstroms from its surface. Solving Poisson's equation for a paraboloid tip with a radius of curvature r_0 and with a voltage U applied with respect to a counterelectrode a distance L away one finds for the field distribution along the symmetry axis of the tip

$$F_z=2U/\ln(1+2L/r_0)(r_0+2z), \tag{5}$$

where z is measured from the surface of the tip. This implies that most of the potential drop occurs within a distance of the radius of curvature of the tip from the tip surface with most of the space towards the counterelectrode being essentially field free. What is reported is either the applied voltage (which does not contain any information about the local field strength without giving simultaneously details about the local tip geometry, etc.) or the externally applied electrostatic field, F, which is the more or less constant field at distances around a few tenths of the tip radius, where the field is essentially constant, i.e., for the model (5) the value at $z=0$. F is usually calibrated against the best image field for neon as imaging gas or evaporation field for the field emitter material.

Tips with a radius of curvature of a few hundred angstroms consist of small regions of low-index crystallographic orientation typically less than 100 Å in diameter separated by steps and faceted regions. Protruding metal atoms in these regions lead to local enhancements of the electric field and serve as preferred sites of field-induced adsorption. Field enhancement also occurs above atoms on the flat regions of the tip as is already apparent classically if we model the adatom by a hemispherical boss of radius R on an otherwise flat metal surface in which case one finds that there is an enhancement of the field given by[18]

$$F_z=4\pi\sigma_0[1+(3z^2/r^2-1)R^3/r^3], \tag{6}$$

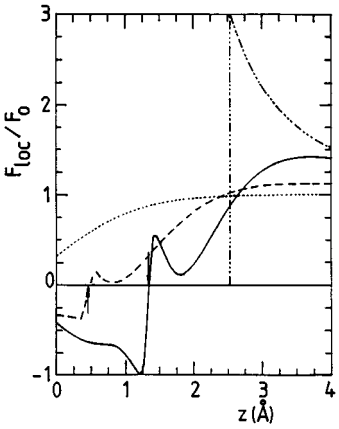

FIG. 6. The field enhancement above a single Li atom on a Li(100) surface [solid line, cluster in Fig. 7(a)], for half a monolayer [dashed line, cluster in Fig. 7(b)], classically for a hemispherical cap (dashed-dotted line) and for a flat jellium surface with $r_s=3.0$ (dotted line). Down arrow points to the adatom; up arrow to the first layer for half a monolayer.

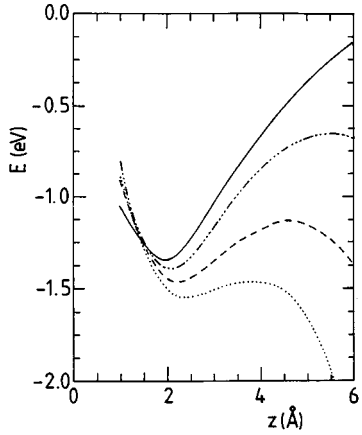

FIG. 8. Potential energy, defined in (7), of a Li adatom as a function of distance perpendicular to the surface for adsorption of a single Li atom on a Li(5+4) cluster, left geometry in Fig. 7, in the CEJ model for $F_0=0$ (solid), 0.5 (dash-dotted), 0.8 (dashed), and 1.0 (dotted) V/Å. The jellium edge is at $z=0$.

where σ_0 is the excess charge laterally far from the protrusion, z is the distance from the surface, and r is measured from the center of the protrusion.

Local-field enhancement also results from a quantum-mechanical treatment of the problem. In Fig. 6 we show the local-field distribution above a single Li atom and above a 2×2 half monolayer of Li adsorbed on a Li cluster embedded in a jellium calculated in the local-density approximation of density-functional theory; the geometry is depicted in Fig. 7. For a flat jellium surface without an adsorbate the field drops gradually from its constant value far from the surface to zero within a few angstroms exhibiting small Friedel oscillations inside the metal; see the dotted curve. The adsorbed atom expels the field further, leading to an additional (positive) charge enhancement on the outside of the atom that results in a field enhancement typically of a factor 1.5–2.0 somewhat smaller than above the classical hemispherical cap and also more smeared out. For the comparison of the classical (dash-dotted curve) and quantum-mechanical calculations we have assumed that the hemispherical cap is centered at the nucleus of the adsorbed atom and has a radius equivalent to its van der Waals radius. The discontinuous surface of the classical metal we put at the centroid of the induced surface charge necessary to create the external field; it is typically a few tenths of an angstrom outside the jellium edge, itself assumed to be half an interlayer separation outside the topmost layer of the underlying crystal structure of the metal. Similar calculations for Rh (Ref. 19) were proved recently in direct measurements of the local-field distributions above individual surface atoms[9] and are in detail reviewed in Ref. 20.

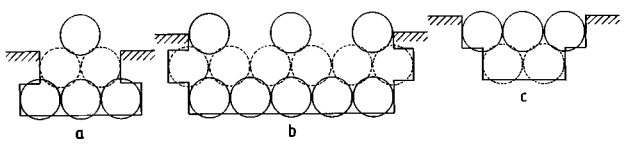

FIG. 7. Geometry of the CEJ model for single adatom (a), half a monolayer (b), and a full monolayer (c). Note the shift in the jellium edge.

IV. THEORETICAL MODEL

We base our calculations of the adsorption of lithium in the presence of high electric field and the local-field enhancement above lithium atoms and clusters on the CEJ (clusters embedded in jellium) model.[21] It was designed to improve the inclusion of field effects in cluster calculations. In the CEJ model one cuts a hole into a semi-infinite jellium to accommodate a cluster of atoms to represent a portion of the metal and any adsorbate one wishes to study; see Fig. 7. After determining the electrostatic field distribution around the hole using density-functional theory[22,23] one imposes this field on the cluster calculating its electronic structure using again density-functional theory, specifically the deMon program.[24]

Figures 1 and 8 have been calculated in the CEJ model. The potential in Fig. 1 is given by

$$V(r;F_0)=E_{\text{total}}(r,F_0;M-A)-E_{\text{total}}(r,F_0;M)-E_{\text{total}}(r,F_0=0;A), \tag{7}$$

where a number of such curves for different field strengths are shown. Its depth at the minimum is the (positive) field binding energy, E_B, i.e., the energy needed to remove an atom or molecule from the adsorbate into field-free space. We note that this energy slightly increases as a function of field strength, which we can explain as a result of including the polarization energy of the adsorbed atom. For $F_0=8$ V/nm, the polarization energy of an isolated Li atom is 0.30 eV, calculated from density-functional theory with nonlocal exchange and correlation energies. The local-field strength near the Li(100) at the equilibrium position of the adsorbed Li atom is about $0.7F_0$; see Fig. 9. Thus the polarization energy of the adatom is about 0.15 eV, while the calculated increase of the binding energy is $E_B(F_0=8$ V/nm$)-E_B(F_0=0)=0.12$ eV. If the polarization energy

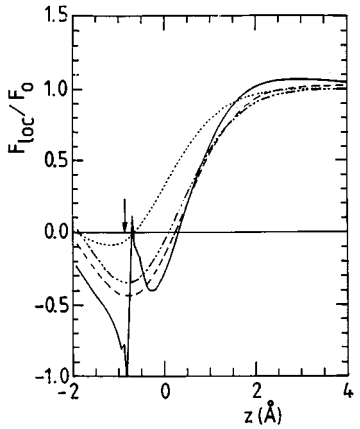

FIG. 9. The field distribution above a Li(100) surface (represented by 9 atoms in the topmost layer and 5 in the next) in the CEJ model along a line through an on-top site (solid line), a bridge site (dashed line), a fourfold hollow site (dashed-dotted line), and for a flat jellium surface with $r_s=3.0$ (dotted line). The arrow gives the position of the topmost lattice plane; $z=0$ is the jellium edge.

were not included one would find that the minimum in the potential would actually go up rather than down as a function of field strength. We note that the deMon programme yields a polarizability $\alpha=0.0135$ nm^3 for a Li atom in good agreement with the experimentally observed trend where the polarizability of Li adatom, which is less than 0.005 nm^3 in Li submonolayer[6,25] increases when thick Li film grows[26] (polarizability of free Li atom 0.02 nm^3 (Ref. 27)].

We next show the field distribution in front of the perfect Li(100) surface on a line perpendicular to it and through on top, bridge, and fourfold hollow site positions; see Fig. 9. The field rises monotonically except on the line through a topmost atom where we find a small enhancement of the field by about 5%. We note that a jellium calculation with $r_0=3.0$ bohr gives similar results. Adding a single Li atom on top the Li(100) surface we get a field enhancement above the adatom due to the fact that at this protrusion the electrons are easier to push into the metal; see Fig. 6. We get a field enhancement of 1.42 some 2.35 Å above the center of the adatom. Li adsorption on a jellium[19,28] with $r_s=3.0$ yields 1.29.

Our next task is to follow the reduction of the field enhancement as one goes from a single adatom to a full monolayer. We model half a monolayer by the cluster depicted in Fig. 7 and show the resulting field enhancement as the dashed line in Fig. 6, amounting to less than 5%.

Before going into detailed comparisons between experiment and theory it is worthwhile to assess the accuracy of the latter. First of all, it is known that the use of the local-density approximation to the exchange and correlation energy typically underestimates the binding energy of dimers by 0.1–0.3 eV. The use of rather small clusters also leads to an overestimate of binding and activation energies of the order of 0.1 eV even if we use nonlocal density-functional theory. As for the chemisorption code of Lang and Williams[28] there is an additional approximation, namely, that the Schrödinger equation is solved only in a sphere of a radius typically some 8 bohr around the adatom. The electronic redistribution outside this sphere is taken into account in a global way by adding a term $e_F dQ_{\rm sph}/e$ to the energy where e_F is the Fermi energy and $dQ_{\rm sph}$ is the net charge of the sphere. The resulting uncertainty in the binding or activation energies is of the order of 0.1 eV.

V. INTERPRETATION OF EXPERIMENTAL RESULTS

On the basis of the CEJ model described in the previous section we now want to interpret the experimental data on (i) the field dependence of the activation energy in Fig. 4, (ii) the dependence of the desorption field on the surface density, Fig. 2, and (iii) the dependence of the binding energy on the externally applied field. It is important to realize that these three sets of data are obtained in kinetic measurements. Although obvious for the activation energy and the desorption field, it is worth repeating that the binding energy is also obtained kinetically namely, from activation and appearance energies, and not e.g., as the equilibrium heat of adsorption from measurements of isotherms or isobars. With an external field applied these would not strictly be equilibrium measurements either but merely done under steady-state conditions, even if surface diffusion is so fast that quasiequilibrium is maintained throughout. The reason why we stress this point is that kinetic data can only be interpreted properly and compared to theoretical modeling if the reaction, i.e., desorption, path is found and specified. The additional point to be discussed for field desorption apart from activation energies is the prefactor, which is controlled to a large extent by the tunneling probability to form an ion.

A. Field desorption of Li at low coverage

In Fig. 4(b) we show the activation energy of field desorption for Li from a submonolayer adsorbed on the [111]-oriented apex plane of W. The fact that the activation energy remains more or less constant for fields larger than 6 V/nm may be due to the fact that measurements were done in the presence of surface diffusion supply that can influence the local coverage, as it was discussed in Ref. 8. Extrapolating desorption field data to zero coverage (Fig. 2) suggests higher initial desorption field for the W(111) surface, than for the W(110), $F_{\rm des}$[Li/W(110)]=8 V/nm and $F_{\rm des}$[Li/W(111)] =10 V/nm, in agreement with general trend observed earlier for other alkalis.[3–5]

We now turn to our calculations. Unfortunately we cannot do calculations for Li on W because the deMon program does not provide basis sets for elements in the sixth row of the periodic table. We have therefore chosen Mo as the substrate that has the same structure, similar lattice constants, and also an ionization energy that is much lower than that of Li. Very close values of the binding energy, and similarity in the surface structures of the alkali adsorbates on the W(hkl) and Mo(hkl) (Ref. 29) give further support to this choice. We first calculated the binding energy of a single Li atom on Mo in zero field. We get for the on-top site on Mo(111) $E_{\rm binding}$[Li-Mo(111)]=2.66 eV. For the evaporation field we calculate $F_{\rm des}$[Li-Mo(111)]=8 V/nm for the on-top site and 11 V/nm for the threefold hollow site in good agreement with the experimental value of the desorption field of Li on W(111), namely, 10 V/nm. In the on-top position the Li atom is adsorbed at a distance where there is some field enhancement whereas in the hollow site the field is already reduced

due to the expulsion from the metal, thus one needs higher applied field to desorb Li adatom. In Fig. 4(b) we show the calculated field dependences of the field-desorption (activation) energy for a single Li atom on the Mo(111) surface for both the on-top and the hollow sites. They bracket the experimental data for Li on W(111). The differences being due to (i) the different substrates, and (ii) the nonzero coverage in the experiment which, for the purpose of this comparison, effectively shifts the scale of the field (in the calculations) to higher values, implying a translation of the theoretical curve to the right.

B. Field desorption of Li from Li monolayer and multilayer

Our next task is to understand the experimental data in Figs. 2(a) and 2(b). Our calculations are in agreement with the experimental value of desorption field [10 V/nm for Li/W(111)] at zero coverage. To follow the coverage dependence of the desorption field up to a full monolayer, accounting for ordered structures as well, is totally beyond the capability of accurate cluster calculations. We therefore have to resort to a few selected geometries to account for the trends in the experimental data.

We first look at field evaporation of a single Li atom on a Li cluster and calculate a desorption field of 11.4 V/nm in perfect agreement with the experimental value for desorption from a second Li layer on W(110); see the lower curve (at 20 K) in Fig. 2(a). This agreement should, however, not be overinterpreted because the calculations are not that accurate in any case. There is also the question of whether desorption from a second layer occurs from isolated atoms or is more akin to evaporation from the solid, i.e., takes place from (self-replicating) kink sites. We should remember that alkali atoms on transition metals experience a strong repulsion at low, submonolayer coverages due essentially to their partially ionic character. Although this repulsion switches to an overall attraction as a monolayer is completed, one can again envisage some ionic character as the first few atoms accumulate in the second layer due to leakage from the substrate. If this were the case then our model would indeed be appropriate.

This scenario would also explain the experimental finding that the evaporation field is smaller for desorption from a second Li layer on top of a (completed) first layer than it is for desorption close to but below a monolayer. Around isolated Li atoms in the second layer field penetration is large, reducing the necessary external field strength, whereas a more or less complete first layer expels the external field very effectively so that a higher field is necessary for the removal of atoms. We have modeled this situation by calculating field desorption from a completed layer, i.e., the removal of the center atom in the right cluster of Fig. 7, and find that a field larger than 20 V/nm is needed to do the job. This is indeed reasonable as an upper bound because desorption from a completed monolayer is very likely a two-step process in which an atom is first transferred into the second layer and then desorbs, a process requiring a smaller field.

In Fig. 4(a) we show the calculated dependences of the desorption (activation) energy for the Li atom adsorbed on a Li(5+4) cluster embedded in jellium and (dashed curve) on the jellium with $r_s=3.0$ bohr in comparison with experimental data for the two-layer Li film.

Because a field of the order of 5 V/nm and larger, can move alkali adatoms on the surface even at temperatures as low as 20 K, the question arises whether rolling motion[11,30] is important for field desorption of Li. Consider the following (rather extreme) situation: we know, e.g., from Fig. 6, that there is a considerable field enhancement above single atoms on a plane. This implies field gradients along which an additional Li atom might migrate until it finally hops on top of the first atom from where it desorbs quite readily. This argument is too simplistic for two reasons: (i) The field gradient is most likely not strong enough to overcome the repulsive interaction between the two Li atoms, and (ii) the field of a single Li atom on the plane (being the appropriate external force for an infinitesimal test charge) gets drastically modified by the presence of a second Li atom reducing the gradients considerably. It is therefore our opinion that the mobility of alkali atoms on field emitters (i) assures an adequate supply of Li at the apex and (ii) also plays the role it does in field-free situations, namely, to maintain the adsorbate in quasiequilibrium.

It is of interest to compare the independently measured field-free coverage dependence of the Li-W(111) (Ref. 17) with present results obtained in high-field conditions. Figure 5 displays such a comparison, where we found the value of 2.05 eV as corresponding to the surface density of 5.9×10^{14} Li atoms per cm^2 [structure (1×1) at 5.7×10^{14} cm^{-2}], and 1.5 eV on the saturated part of the binding energy curve as expected from the ''monolayer'' and ''second layer'' field-desorption modes realized in our experiments. The field independence of the binding energy of Li for different Li coverages found in present experiments seems at first glance to be in discrepancy with the recently observed field dependence of the binding energy of field-evaporated Rh.[11] However, the essential difference in binding mechanisms of Rh to its own lattice and of Li to the W(111) surface and the resulting difference in applied fields necessary for field evaporation of Rh [41 V/nm (Ref. 11)] and for field desorption of Li from W (4–10 V/nm), leads to a difference in the field-induced charge transfer. The expected variations of the Li binding energy caused by an applied field less than 10 V/nm, lie within the experimental accuracy of the present work (0.1 eV) limited by the activation energy measurements. A direct comparison of the alkali adsorption-induced electronic perturbations[31,32] with calculations of the electron density redistribution near a metal surface, caused by the applied electrostatic field[33] give further support to these conclusions.

VI. SUMMARY

In summary, we have presented a method for the derivation of binding energies of alkali adatoms on metal surfaces from the measurements of absolute appearance energies for field-desorbed alkali ions and of the activation energy of field desorption. Field-independent values of the binding energy of Li adatoms in the Li monolayer and in second Li layer on W(111), which were obtained from the thermionic cycle using field-dependent values of $A_{\mathrm{Li}}(F)$ and $Q(F)$, are in agreement with results of field-free measurements for a W(111) single-crystal plane.

We have used the CEJ model, based on density-functional theory, to calculate self-consistently the local-field enhance-

ment, surface potentials, and activation energies for field desorption as a function of field strength and surface coverage and geometry. A consistent interpretation of the experimental data emerges in which the local-field enhancement and field penetration play a crucial role.

ACKNOWLEDGMENTS

We thank M. Naschitzki for his excellent technical assistance. The Max-Planck-Gesellschaft is acknowledged for financial support of one of us (V.K.M.). This work was supported in part by a grant from the Office of Naval Research.

*Author to whom correspondence should be addressed. On leave from Technical University of Lviv, Lviv/Ukraine.

†On leave from Institute of Physics, National Academy of Sciences, Kiev, Ukraine.

[1] E. W. Müller, Naturwissenschaften **29**, 533 (1941).

[2] E. W. Müller, Phys. Rev. **102**, 618 (1956).

[3] C. J. Todd and T. N. Rhodin, Surf. Sci. **42**, 109 (1974).

[4] A. G. Naumovets, Fiz. Tverd. Tela **5**, 2294 (1963) [Sov. Phys. Solid State **5**, 1668 (1964)].

[5] K. Sendecka and R. Meclewski, Surf. Sci. **70**, 255 (1978), and references therein.

[6] Yu. Suchorski, Surf. Sci. **247**, 346 (1991).

[7] Yu. Suchorski, V. K. Medvedev, J. H. Block, and H. J. Kreuzer (unpublished).

[8] Yu. Suchorski, V. K. Medvedev, and J. H. Block, Phys. Rev. B **51**, 4734 (1995).

[9] W. A. Schmidt, N. Ernst, and Yu. Suchorski, Appl. Surf. Sci. **67**, 101 (1993); N. Ernst, *ibid*. **67**, 82 (1993).

[10] W. A. Schmidt, Yu. Suchorski, J. H. Block, H. J. Kreuzer, and R. L. C. Wang, Surf. Sci. **326**, 243 (1995).

[11] W. A. Schmidt and N. Ernst, Vacuum **45**, 255 (1994).

[12] V. K. Medvedev, Yu. Suchorski, and J. H. Block, Ultramicroscopy **53**, 27 (1994).

[13] T. T. Tsong, W. A. Schmidt, and O. Frank, Surf. Sci. **65**, 109 (1977).

[14] E. W. Müller and T. T. Tsong, *Progress in Surface Science* (Pergamon, Oxford, 1973), Vol. 4, Pt. 1.

[15] N. Ernst, Surf. Sci. **87**, 469 (1979).

[16] R. G. Forbes, Surf. Sci. **61**, 221 (1976).

[17] V. K. Medvedev and T. P. Smereka, Fiz. Tverd. Tela **16**, 1599 (1974) [Sov. Phys. Solid State **16**, 1046 (1975)]; V. K. Medvedev and A. I. Yakivshuk (unpublished).

[18] D. J. Rose, J. Appl. Phys. **27**, 215 (1956).

[19] H. J. Kreuzer, L. C. Wang, and N. D. Lang, Phys. Rev. B **45**, 12 050 (1992).

[20] Yu. Suchorski, W. A. Schmidt, N. Ernst, J. H. Block, and H. J. Kreuzer, Prog. Surf. Sci. **48**, 121 (1995).

[21] R. L. C. Wang and H. J. Kreuzer (unpublished).

[22] N. D. Lang and W. Kohn, Phys. Rev. B **1**, 4555 (1970); **3**, 1215 (1971); **7**, 3541 (1973).

[23] N. D. Lang, in *Solid State Physics*, edited by F. Seitz, D. Turnbull, and H. Ehrenreich (Academic, New York, 1973), Vol. 28, p. 225.

[24] A. St-Amant, Ph.D. thesis, Universite de Montreal, 1992; A. St-Amant and D. R. Salahub, Chem. Phys. Lett. **169**, 387 (1990).

[25] E. V. Klimenko and A. G. Naumovets, Fiz. Tverd. Tela. (Leningrad) **13**, 33 (1971) [Sov. Phys. Solid State **13**, 25 (1971)].

[26] A. G. Naumovets, Fiz, Tverd. Tela. (Leningrad) **6**, 2088 (1964) [Sov. Phys. Solid State **6**, 1647 (1965)].

[27] A. Dalgarno, Adv. Phys. **2**, 484 (1962).

[28] N. D. Lang and A. R. Williams, Phys. Rev. B **18**, 616 (1978).

[29] A. G. Naumovets, in *The Chemical Physics of Solid Surfaces and Heterogeneous Catalysis*, edited by D. A. King and D. P. Woodruff (Elsevier, Amsterdam, 1993), Vol. 7.

[30] R. Wough, E. D. Boyes, and M. J. Southon, Surf. Sci. **61**, 109 (1976).

[31] N. D. Lang, Surf. Sci. **299/300**, 284 (1994), and references therein.

[32] P. J. Feibelman and D. R. Hamann, Surf. Sci. **149**, 48 (1985).

[33] P. Gies and R. R. Gerhardts, Phys. Rev. B **33**, 982 (1986); F. Schreier and R. Rebentrost, J. Phys. C **20**, 2609 (1987); G. G. Aers and J. E. Inglesfield, Surf. Sci. **217**, 367 (1989).